Molecular Dynamics Study of Dielectric Properties of Water−Dimethyl Sulfoxide Mixtures

Munir S. Skaf†

Instituto de Química, UNICAMP, Cx.P. 6154, Campinas, SP 13083-970, Brazil

Received: June 30, 1999; In Final Form: October 5, 1999

Both the static and dynamic dielectric properties of water−dimethyl sulfoxide (DMSO) mixtures over the whole composition range are investigated by means of molecular dynamics (MD) simulations, and the results are compared with available experimental measurements. We discuss the behavior of the dielectric constant and Kirkwood dipole correlation factor as functions of composition in terms of the self- and cross-species dipole density correlations and a suitable set of real space dipole−dipole distribution functions. We find that short-ranged structural correlations between neighboring water and DMSO molecules strongly influence the system's static dielectric properties, as expected on the basis of the molecular associations these mixtures are known to exhibit. In terms of the dynamics, we report time correlation functions for the mixtures' dipole densities and find that their long-time behavior can be reasonably well described by either biexponential or stretched exponential decays, which means that the dielectric relaxations of these mixtures are governed by complex, multi time scale mechanisms of rotational diffusion. The dipole density relaxation time is a nonmonotonic function of composition passing through a maximum around 33% mole DMSO, in agreement with the experimental data for the mixtures' main dielectric relaxation time. Frequency-domain results such as the frequency spectra of the single-dipole time correlations and the experimentally accessible far-infrared absorption coefficient reveal that mixing also exerts a profound effect upon the librational dynamics of water molecules. This effect is much stronger than and qualitatively different from that observed in other associating aqueous mixtures and has been examined in view of new DMSO−water molecular aggregates suggested in previous MD works.

I. Introduction

The prominent hydrophilic nature of DMSO makes it capable of forming strong and persistent hydrogen (H)-bonds to water through its oxygen atom.[1−4] This leads to the formation of DMSO−water molecular aggregates of well-defined geometry which are often held responsible for the strong nonideal mixing behavior manifested as maxima or minima in several physicochemical properties.[5−11] The largest deviations from ideal mixing occur around 33% mole DMSO, thus suggesting the existence of stoichiometrically well-defined 1DMSO:2water "complexes". These molecular associations seem to be important to the behavior of these mixtures at the liquid−vapor interface as well.[12,13]

Recently, a number of molecular dynamics (MD) simulations[4,14−16] and neutron diffraction experiments[15] have indeed identified the structure of the 1DMSO:2water complex and linked many of the structural and dynamical features of DMSO−water mixtures to the presence of such aggregates. More recently, Borin and Skaf[16] have found from MD simulations a second, distinct type of aggregate consisting of two DMSO linked by a central water molecule through H-bonding, which is expected to be the predominant form of molecular association between DMSO and water in DMSO-rich mixtures. This H-bonded complex is referred hereby as 2DMSO:1water aggregate. From the dynamical point of view, both the translational and rotational motions, as indicated by NMR[8−10,17] and dielectric relaxation data,[11] seem to be strongly coupled and considerably slower than the pure liquids' motions at compositions around 33% DMSO. This behavior is markedly in contrast with that exhibited by other H-bonding liquids such as water−methanol, water−ammonia, and water−acetone mixtures.[18]

The dielectric behavior is one of the key ways of characterizing polar liquid environments as reaction media. Experimental measurements have been available for some time for the composition dependence of the dielectric constant and dielectric relaxation of DMSO−water mixtures,[11] but a detailed microscopic study of these properties is still lacking. One notable exception is the early work by Luzar, who presents a mean-field theory for the dielectric constant of these mixtures, highlighting the importance of H-bonding to the excess dielectric constant.[19] In the H-bonding methanol−water mixtures, molecular dynamics (MD) simulation studies[20,21] have led to valuable molecular-level insights, showing that both the static[20] and dynamic[21] dielectric behaviors are consistent with the singular structural and dynamical properties of the H-bond network.[18] These studies were particularly revealing in connection to the high-frequency modes of dielectric relaxation where librational and inertial dynamics dominate. In this frequency range, the analytical dynamical theories[22,23] based on Stockmayer-like potentials are less applicable.

In view of the above, we have undertaken a series of extensive MD simulations in order to investigate the dielectric properties of DMSO−water mixtures from a microscopic point of view over the entire composition range. With this aim, results for static properties such as the dielectric constant, Kirkwood dipole correlation factor, and the pertinent dipolar symmetry projections[24] $h^{110}(r)$ have been calculated in addition to several dynamical properties using well-established interaction site potentials for water and DMSO. For the dynamics, we calculated time autocorrelation functions for the $k = 0$ dipole densities, as

† E-mail: skaf@iqm.unicamp.br.

10.1021/jp992247s CCC: $18.00
Published on Web 11/19/1999

well as for their transverse and longitudinal components at the smallest wave vectors in the systems. Analysis of dielectric properties at finite wave vectors have been used to reveal to which extent the simulated system sizes are representative of the thermodynamic limit as far as the dielectric properties are concerned. The relaxation of the longitudinal dipole density at the smallest k is also investigated in some detail because of its connection with the solvation dynamics response,[25] which have been very recently studied in these mixtures through MD simulations.[26,27] To gain insight about the self-species and interspecies correlations, the mixture dipolar relaxation has been calculated in terms of the separate contributions from each molecular species and the DMSO−water cross-correlations. In addition, we have also calculated and discussed the mixture's frequency-dependent far-infrared (FIR) absorption coefficient.[28]

In the next section, we present the potentials and simulation details, and summarize the results of linear response theory relating the dielectric permittivity tensor to the dipole density correlation functions. In section III, we present the results for the static dielectric properties. The results for the dipole density time correlations functions are presented in section IV, while the frequency spectra are discussed in section V. Concluding remarks are found in section VI.

II. Simulation Details and Theoretical Formulation

A. Models and Simulations. We have considered here mixtures with DMSO mole fractions $x_D = 0.13$, 0.35, 0.50, 0.66, and 0.81, as well as the pure liquids at ambient conditions. For water we have used the well-known SCP/E model,[29] while for DMSO we used the four-site P2 potential of Luzar and Chandler,[4] where each methyl group is treated as a single site. The intermolecular potentials are described by site−site interactions given by a sum of Lennard-Jones plus Coulomb terms. The Lennard-Jones parameters for sites of different types are set by the usual Lorentz−Berthelot combining rules, $\epsilon_{ij} = \sqrt{\epsilon_{ii}\epsilon_{jj}}$ and $\sigma_{ij} = (\sigma_{ii} + \sigma_{jj})/2$. This procedure has been used in other simulations of aqueous mixtures, including DMSO−water mixtures, with relative success. Site parameter and molecular geometries are found in ref 4 (DMSO) and ref 29 (water). Some calculated properties for these models may be found in refs 30 and 31a.

The simulations were performed on the NVE ensemble with 500 molecules placed in cubic boxes with periodic boundary conditions at 298 K. The numbers of DMSO molecules corresponding to the mixtures approximately at 13, 35, 50, 66, and 81% DMSO are 65, 175, 250, 330, and 405, respectively. The pure water simulations were run using 256 molecules. In each case, the box dimensions were chosen so as to match the corresponding experimental densities[6] at 298 K and 1 atm. The Lennard-Jones forces were cut off at half the box length, while Ewald sums with conducting boundaries[32] were applied to the long-ranged portions of the electrostatic forces. The equations of motion were integrated using the leapfrog[33] algorithm with a time step of 3 fs, while the molecular geometries were restored using SHAKE.[34] For pure DMSO the time step was 6 fs. This enabled total energy conservation within 0.5% error during uninterrupted production runs lasting about 12 ps for each mixture and 24 ps for pure DMSO. Approximately 200 such runs were performed for each simulation stated, performing a total of 2.5 ns trajectories for each system (4 ns for pure DMSO). The production runs were intercalated by smaller (4 ps) runs during which the velocities were rescaled according to the desired temperature. Before the production runs, each mixture was equilibrated during 100 ps starting from an fcc lattice over which water and DMSO molecules were initially randomly distributed. Water and DMSO density profiles were also calculated after equilibration to ensure the system was homogeneous throughout.

B. Linear Response Theory of Dielectric Relaxation. For the simulated systems, the longitudinal (L) and transverse (T) components of the (external field-independent) electric susceptibility, χ, and dielectric permittivity tensors are related through[32,33]

$$\chi_L(\mathbf{k},\omega) = 1 - \epsilon_L^{-1}(\mathbf{k},\omega) \tag{1a}$$

and

$$\chi_T(\mathbf{k},\omega) = \epsilon_T(\mathbf{k},\omega) - 1 \tag{1b}$$

Considering only contributions from the molecular dipoles, the linear response susceptibility is given by[35,36]

$$\chi_A(\mathbf{k},\omega) = 9y\frac{\langle|\mathbf{M}_A(\mathbf{k},0)|^2\rangle}{\nu_A N\mu^2}[1 + i\omega\Phi_A(\mathbf{k},\omega)] \tag{2}$$

where y is the dipolar strength of the mixture

$$y = \sum_\alpha y^\alpha \qquad y^\alpha = \frac{\rho^\alpha \mu_\alpha^{\,2}}{9k_B T\epsilon_o} \tag{3}$$

with $\rho^\alpha = N^\alpha/V$ being the number density of species α, μ_α the magnitude of its dipole, and $\mu^2 = x_d\mu_d^2 + x_w\mu_w^2$ defines an average squared dipole. The subscript A = L or T for the longitudinal and transverse components, and ν_A takes on the values $\nu_L = 1$ and $\nu_T = 2$. The function $\Phi_A(\mathbf{k},\omega)$ is the Fourier transform

$$\Phi_A(\mathbf{k},\omega) = \int_0^\infty dt\, \Phi_A(\mathbf{k},t)\exp(i\omega t) \tag{4}$$

of the normalized dipole density correlation function

$$\Phi_A(\mathbf{k},t) = \frac{\langle\mathbf{M}_A(\mathbf{k},t)\cdot\mathbf{M}_A(-\mathbf{k},0)\rangle}{\langle|\mathbf{M}_A(\mathbf{k},0)|^2\rangle} \tag{5}$$

$\mathbf{M}(\mathbf{k},t)$ is the spatial Fourier transform of the system's dipole density:

$$\mathbf{M}(\mathbf{k},t) = \sum_\alpha\sum_{j=1}^{N^\alpha}\mu_\alpha^j(t)\exp[i\mathbf{k}\cdot\mathbf{r}_\alpha^j(t)] = \mathbf{M}^d(\mathbf{k},t) + \mathbf{M}^w(\mathbf{k},t) \tag{6}$$

where μ_α^j is the dipole moment of the jth molecule of species α and $\mathbf{r}_\alpha^j(t)$ is the position of its center of mass with respect to the lab frame. According to eq 6, the mean-squared dipole density has contributions from the dipole density self-correlations for each molecular species plus the inter-species cross-correlations:

$$\Phi_A(\mathbf{k},t) = \Phi_A^{dd}(\mathbf{k},t) + \Phi_A^{dw}(\mathbf{k},t) + \Phi_A^{ww}(\mathbf{k},t) \tag{7}$$

where

$$\Phi_A^\alpha(\mathbf{k},t) = \frac{\langle\mathbf{M}_A^\alpha(\mathbf{k},t)\cdot\mathbf{M}_A^\alpha(-\mathbf{k},0)\rangle}{\langle|\mathbf{M}_A(\mathbf{k},0)|^2\rangle} \qquad \text{with} \qquad \alpha = d, w \tag{8a}$$

and

$$\Phi_A^{dw}(\mathbf{k},t) = 2\frac{\langle \mathbf{M}_A^d(\mathbf{k},t)\cdot\mathbf{M}_A^w(-\mathbf{k},0)\rangle}{\langle |\mathbf{M}_A(\mathbf{k},0)|^2\rangle} \quad (8b)$$

Because of the periodic boundary conditions the wave vectors are of the form

$$\mathbf{k} = (l,m,n)\frac{2\pi}{B} \quad (9)$$

where l, m, and n are integers and B is the length of the cubic box for each mixture.

The $\mathbf{k} \equiv 0$ permittivity for a simulated system using Ewald with conducting boundaries is[36]

$$\epsilon(\omega) = 1 + 9y\frac{\langle |\mathbf{M}(0)|^2\rangle}{3N\mu^2}[1 + i\omega\Phi(\omega)] \quad (10)$$

where $\Phi(\omega)$ and $\mathbf{M}(t)$ are given by eqs 4−6 with $\mathbf{k} \equiv 0$. For the system sizes we have used, the limiting procedure $\epsilon(\omega) = \lim_{k\to 0}\epsilon_T(k,\omega)$ can be reached at $\mathbf{k} = \mathbf{k}_1$ (the smallest wave vector attainable in the system) within the statistical accuracy of our results.

A more detailed comparison between simulated and experimentally measured dipolar relaxation of high-frequency motions can be obtained through the far-IR absorption coefficient:

$$\alpha(\omega) = \frac{[\epsilon(0) - 1]\omega^2}{n(\omega)c}\frac{\tanh(\beta\hbar\omega/2)}{\beta\hbar\omega/2}\int_0^\infty \Phi(t)\cos(\omega t)\,dt \quad (11)$$

where $n(\omega)$ is the frequency-dependent refractive index and c is the speed of light in a vacuum. The dielectric constant $\epsilon(0)$ and the $\Phi(t)$ correlation function can be evaluated at $\mathbf{k} = 0$ or at the smallest nonzero wave vector allowed in the simulations, according to procedures described elsewhere.[21] Equation 11 also incorporates some approximated quantum corrections to the absorption coefficient, which are important at the librational frequencies of water. Different approximations can be used to incorporate quantum effects in the spectra of classical correlation functions.[37] We have chosen this particular one because it yields good agreement between the experimental and simulated far-IR absorption coefficients for water using the SPC and SPC/E models.[38]

The static dielectric properties are obtained from eqs 1, 2, and 10 setting $\omega = 0$. In addition to the dielectric constant $\epsilon(0)$, the Kirkwood g factor, g_K, is an experimentally relevant quantity that can be obtained from our simulations through the relation[36]

$$g_K = \frac{[\epsilon(0) - 1][2\epsilon(0) + 1]}{9y\epsilon(0)} \quad (12a)$$

Unlike $\epsilon(0)$, the separate contributions to g_K from the self-species and interspecies correlations cannot be obtained from this equation because of its nonlinearity. Alternative strategies have been used for this purpose in methanol−water mixtures.[20,21] Here, because of the large values of the system's dielectric constant ($40 < \epsilon(0) < 75$), an approximation for the separate contributions can be obtained from eq 12a evaluated at $\mathbf{k} = 0$.

$$g_K \approx g_K^{dd} + g_K^{wd} + g_K^{ww} = \frac{2}{3N\mu^2}\{\langle \mathbf{M}^d\cdot\mathbf{M}^d\rangle + 2\langle \mathbf{M}^w\cdot\mathbf{M}^d\rangle + \langle \mathbf{M}^w\cdot\mathbf{M}^w\rangle\} \quad (12b)$$

Also of interest here are the dipolar symmetry projections $h^{110}(r)$ of the pair correlation $h(i,j)$, which can also be conveniently decomposed into self-species and interspecies contributions:[36]

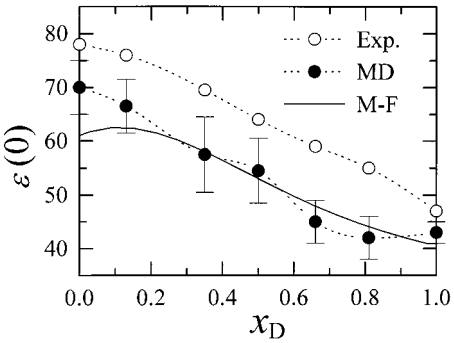

Figure 1. MD (full symbols), experimental[11] (open symbols), and mean-field results[19] (solid line) for the mixture's dielectric constant vs DMSO mole fraction. The dotted lines are drawn as guides to the eye.

$$h^{110}(r) = \sum_{\alpha,\beta}\frac{x_\alpha x_\beta \mu_\alpha \mu_\beta}{\mu^2} h_{\alpha\beta}^{110}(r) \quad (13a)$$

$$h_{\alpha\beta}^{110}(r) = \langle \hat{u}_i^\alpha\cdot\hat{u}_j^\beta\, h_{\alpha\beta}(i,j)\rangle \quad (13b)$$

where $\hat{u}_i^\alpha$ is the unit vector along the dipole of the ith molecule of species α.

III. Static Dielectric Properties

We begin our analysis by presenting the results for the dielectric constant $\epsilon(0)$ as a function of the composition, which is depicted by solid symbols in Figure 1 along with the experimental values from Kaatze et al.[11] (open symbols). The MD data shown have been evaluated from the $\mathbf{k} \equiv 0$ correlations (eq 10 at $\omega = 0$), and the error bars were estimated using the blocking method of Flyvbjerg and Petersen.[39] Considering that the intermolecular potentials used here lack any polarizability effects beyond the usual dipole moment enhancement[30] and the fact that the SPC/E underestimates water's dielectric constant by about 10%,[40] the MD values of $\epsilon(0)$ for the mixtures as well as the trend with composition compare fairly well with the experimental data. It is expected that electronic polarization local field corrections,[36,41] when taken into account, would improve the agreement between MD and experimental data significantly. Also shown in Figure 1 are the mean-field theory results from ref 19 (solid line) with the maximum number of DMSO−water H-bonds fixed at 3. Despite its simplicity, the mean-field treatment reveals the importance of H-bonding to the dielectric constant of this mixture. Around 35 and 50% DMSO, the agreement between the mean-field and simulated dielectric constants seems to be somewhat better than for other compositions. This result may be fortuitous, but it is interesting to notice that good agreement is also found for the average number of DMSO−water and water−water H-bonds predicted by the theory and the MD simulations[4,16] around these compositions.

It is important to stress how converged the present calculations are. The notoriously slow convergence of dielectric properties springs from the well-known fact that they depend on the long-ranged, collective fluctuations of the dipolar polarization. The cumulative averages of the $\mathbf{k} = 0$ dielectric constant and of the transverse component at the smallest wave vector for the different mixtures are shown in Figure 2 as functions of the simulated time. The convergence at nonzero k (dashed lines) is considerably faster, as discussed elsewhere.[21,41,42] The values for the $\epsilon(0)$ and $\epsilon_T(k_1,0)$ are, however,

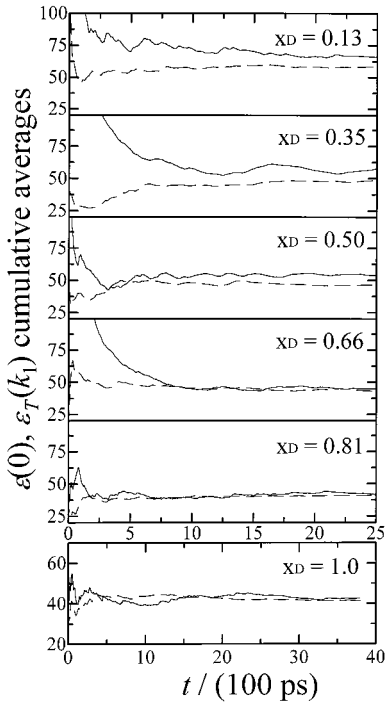

Figure 2. Cumulative averages of the $k = 0$ dielectric constant $\epsilon(0)$ and the transverse component $\epsilon_T(k,0)$ at the smallest nonzero wavevector over the entire simulation length for each mixture and for pure DMSO.

TABLE 1: Dielectric Constant, Kirkwood *g* Factor, and Its Self-Species and Interspecies Contributions for DMSO−Water Mixtures Obtained from MD Simulations[a]

x_D	y	μ/D	$\epsilon(0)$	g_K[b]	g_K^{dd}	g_K^{wd}	g_K^{ww}
0.00	6.25	2.35	70 ± 4	2.45			2.45
0.13	6.18	2.73	66 ± 6	2.37 (2.15)	0.26 (0.57)	0.43	1.68 (1.58)
0.35	6.08	3.26	57 ± 6	2.10 (1.90)	0.70 (1.07)	0.71	0.70 (0.83)
0.50	5.98	3.58	55 ± 5	2.00 (1.80)	1.00 (1.27)	0.62	0.40 (0.53)
0.66	5.89	3.90	45 ± 5	1.68 (1.71)	1.08 (1.41)	0.44	0.15 (0.30)
0.81	5.82	4.17	42 ± 5	1.58 (1.66)	1.25 (1.51)	0.23	0.07 (0.15)
1.00	5.79	4.48	43 ± 4	1.62	1.62		

[a] The quantities in parentheses are the ideal values from eq 14. Also shown are the averaged dipoles and the dipolar strengths. [b] The percentage error of g_K follows the corresponding percentage error of $\epsilon(0)$ (i.e., ∼10%).

close to each other, indicating that the system sizes used in our simulations are representative of the liquid models in the thermodynamic limit.

Let us now focus on the mixture's dipole orientational Kirkwood *g* factor, g_K, and its separate contributions from water, DMSO, and the interspecies cross-correlations, which are hardly accessible experimentally. Table 1 shows the values obtained for g_K and the separate g_K^{dd}, g_K^{wd}, and g_K^{ww} contributions (eq 12b), along with the average squared dipole and the dipolar strength of each mixture. Also shown are the values for the mixtures dielectric constant. The results show that the mixture's Kirkwood *g*-factor decreases nearly monotonically with increasing concentration of DMSO by ∼40%, while the dipolar strength *y* decreases by at most 7% within the composition range considered here. Therefore, the observed decrease in the mixture's dielectric constant with χ_D stems essentially from a decrease in the total dipole−dipole correlation embodied in g_K rather than a decrease in the dipolar strength of the mixture. Such a decrease in g_K is not unexpected here since one of the components (DMSO) is a nonassociating liquid,[31,43,44] with $g_K^{DMSO} \approx 1.60$, as obtained for the P2 potential (see also ref 31a). This behavior is in contrast with that presented by

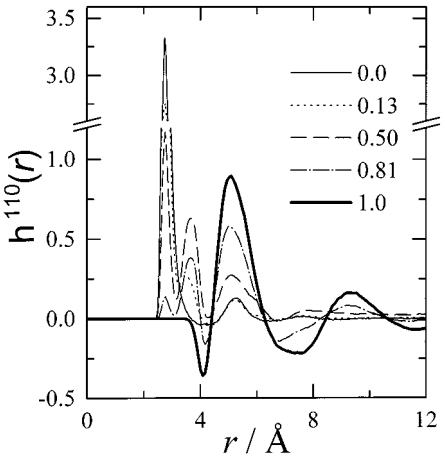

Figure 3. Dipolar symmetry projections $h^{110}(r)$ for all simulated systems. The curves are labeled according to their DMSO mole fraction.

methanol−water mixtures, where g_K is found to be quite insensitive to composition, and the changes in the dielectric constant are mostly due to the variation of the dipolar strength of the mixture.[20,21]

In the absence of interspecies correlations, the mixture's ideal Kirkwood *g* factor would be related to the pure liquids' values, g_K^{DMSO} and g_K^{water}, through the equation

$$g_{id} = g_{id}^{D} + g_{id}^{W} = \frac{x_D \mu_D^2}{\mu^2} g_K^{DMSO} + \frac{x_w \mu_w^2}{\mu^2} g_K^{water} \qquad (14)$$

The values of g_{id}, g_{id}^{D}, and g_{id}^{W} are shown within parentheses in Table 1. Table 1 shows that the self-species contributions g_K^{dd} and g_K^{ww} increase monotonically with x_D and x_W, respectively, while the interspecies cross-correlation g_K^{wd} goes through a maximum at 35% DMSO. Comparison with the ideal values indicate that mixing reduces the self-species contributions below g_{id}^{D} and g_{id}^{W}, while the dipole−dipole correlation between water and DMSO is enhanced to a maximum at 35% DMSO. One interesting point is that at 13% DMSO $g_K^{ww} > g_{id}^{W}$, showing an enhancement in the dipole−dipole correlation between water molecules due to this addition of DMSO. Another point worth mentioning is the fact that at ∼80% DMSO, the mixture's g_K is somewhat smaller than g_K^{DMSO}. Despite the large error bars of these quantities, this suggests that adding some water into DMSO may introduce a higher degree of antiparallel alignment of DMSO dipoles in the mixture. Experimental evidence of this effect was presented by Kaatze et al.[11]

To understand how the behavior described above actually comes about in terms of the liquid's intermolecular structure, let us investigate how the dipolar symmetry projection $h^{110}(r)$ and its contributions $h_{\alpha\beta}^{110}(r)$ (eq 13) evolve with composition as one goes from a water-like to DMSO-like structure upon increasing values of x_D. The results for the total $h^{110}(r)$ are depicted in Figure 3 (the curves are labeled according to the mixture's DMSO mole fraction). The data for pure water (solid line) exhibit a sharp first peak and is positive for essentially all values of *r*, indicating that water has a large Kirkwood *g*-factor, a result due to the well-known strong directionality of the H-bonds between water molecules. DMSO, on the other hand (thick line), presents a negative well at the shortest intermolecular separations, indicative of the antiparallel dipole orientations between nearest neighboring DMSO molecules.[31] Thus, as we have shown in Table 1, g_K^{DMSO} turns out much smaller than g_K^{water} despite the fact that the dipole moment of DMSO is twice as large as water's. For the mixed solvents, the conspicu-

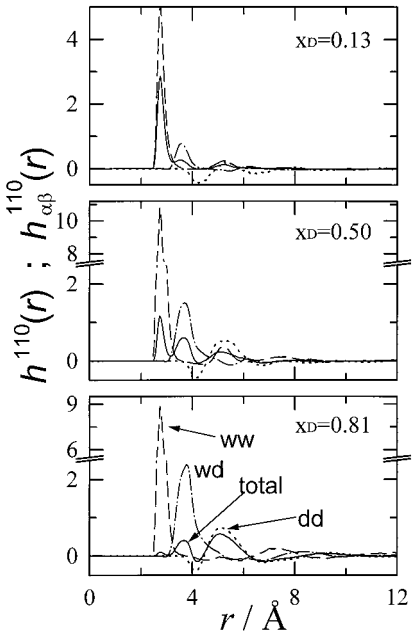

Figure 4. Dipolar symmetry projections $h^{110}(r)$ and their self-species and interpecies contributions $h^{110}_{\alpha\beta}(r)$ for selected mixtures. The labels and line styles in the bottom panel apply to all three panels.

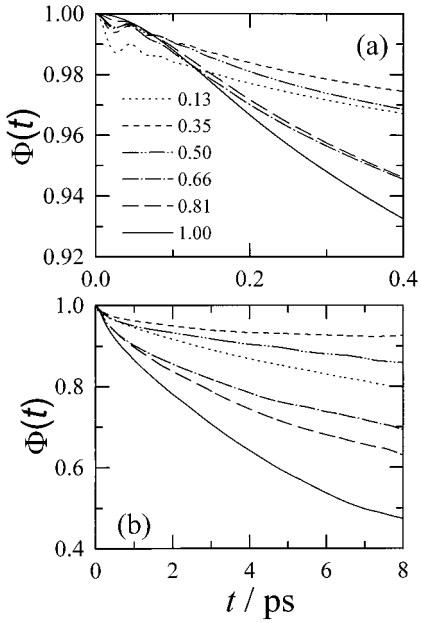

Figure 5. Normalized $k = 0$ dipole density correlations $\Phi(t)$ vs time for all simulated systems (b) and details of the short-time behavior (a).

ous feature is the development of a pronounced peak between 3.5 and 4 Å, which is not present in either of the pure liquids' $h^{110}(r)$ projections. This points to the role of the cross-correlations in this range of intermolecular separations, which can be fully appreciated from the data displayed in Figure 4 for three selected mixtures: water-rich (top panel), equimolar (middle panel), and DMSO-rich (bottom panel). The DMSO self-contribution, $h^{110}_{dd}(r)$ (labeled "dd"), indicates that the relative orientation between DMSO molecules in the pure liquid is well preserved even for the smallest DMSO concentration considered here. Similar considerations holds for the $h^{110}_{ww}(r)$ (labeled "ww") contribution, but in this case the main peak intensity is sharply enhanced as the concentration of DMSO increases. The prominent positive peak between 3.5 and 4 Å in the cross-species contribution, $h^{110}_{wd}(r)$ (labeled "wd"), results from the relative orientation between the dipoles of a neighboring pair of water and DMSO molecules, which lye on a less than 90° angle relative to each other, in agreement with the structure of the 1DMSO:2water aggregates identified by means of MD simulations,[4,14,16] and also by neutron diffraction experiments.[15] For DMSO-rich mixtures, our previous MD simulations[16] have indicated that water and DMSO are predominantly associated through aggregates of composition 2DMSO:1water, whose geometry resembles the 1:2 aggregates, but with water and DMSO molecules interchanged. These aggregates also contribute to the positive peak of $h^{110}_{wd}(r)$ shown in Figure 4, but as we shall see later, their main effects are manifest in the high-frequency librational molecular motions.

IV. Dipole Density Time Correlations

A. $k = 0$ Correlations. We begin our discussion of the dynamical dielectric properties with the $k = 0$ normalized dipole density time correlation functions $\Phi(t)$ for each mixture and for pure DMSO, which are depicted in Figure 5. The curves are labeled according to the DMSO mole fraction x_D. We discuss first their short time behavior (Figure 5a). At very early times (from 0 to 0.02 ps), the $\Phi(t)$ functions exhibit an inertial (or Gaussian) decay that is faster for water-richer mixtures because of water's small moments of inertia. After this initial inertial decay, the functions $\Phi(t)$ show fast damped oscillations associated with the H-bonding librational oscillations characteristic of high torque, associating liquids.[30] These librational oscillations are significantly more prominent for water-richer mixtures since water forms on the average four H-bonds while pure DMSO forms none. Such short-time dynamics cannot be very well appreciated from the time-dependent $k = 0$ (or from the transverse components) dipolar relaxation because slow rotational-diffusion processes dominate its decay. Nevertheless, these fast dynamics give rise to prominent, high-frequency peaks in the far-IR spectra, as discussed later on. Figure 5b, on the other hand, reveals the dramatic effect of the addition of water upon the long time dynamics of DMSO and vice versa. The results shown in Figure 5b indicate that the dipole density correlations are slowly decaying functions, but their overall decay patterns do not follow a simple composition dependence. In can be seen in Figure 5b that pure DMSO (solid line) is more relaxed than all mixtures, but it is still considerably less relaxed than pure water, the fastest of all systems considered (data not shown). This interesting behavior correlates well with the fact that the molecular diffusion and long-time single-particle reorientation processes slow upon mixing.[8-10,16]

Analysis of the long time ($t \geq 0.6$ ps) portions of $\Phi(t)$ (Figure 5b), which characterize the slow diffusional relaxation regime of the dipolar correlations, provides dielectric relaxation time parameters that are valuable quantities to be compared against experimental measurements. Associating polar liquids such as alcohols and alcohol−water mixtures usually present multiple time scales in their dielectric relaxation,[21,45-47] which are often well described by a sum of exponentials with different time constants, indicating a multiple Debye-like behavior, or by a stretched exponential form,[47] which have also been used to describe the reorientational relaxation in liquids near a glass transition.[48] For DMSO−water mixtures, we find that either biexponential or stretched exponential functions provide good fits to $\Phi(t)$ (Figure 5b) at long times, i.e.,

$$\Phi(t) = a_1 \exp(-t/\tau_1) + a_2 \exp(-t/\tau_2)$$

$$\Phi(t) = a_0 \exp[(-t/\tau_0)^{\beta}] \qquad t > 0.6 \text{ ps} \quad (15)$$

TABLE 2: Fits to the Normalized Dipole Density Time-Correlation Functions $\Phi(k = 0,t)$ in the Postlibrational Regime

	biexponential fits				stretched exponential fits		
x_D	a_1	τ_1/ps	a_2	τ_2/ps	a_0	τ_0/ps	β
0.13	0.03	1.8	0.95	48.0	0.98	54.0	0.84
0.35	0.03	1.3	0.95	191.0	0.98	940.0	0.54
0.50	0.04	6.0	0.92	88.8	0.99	518.3	0.49
0.66	0.12	3.3	0.85	55.1	1.00	58.6	0.61
0.81	0.20	3.2	0.76	35.8	0.97	19.8	0.84
1.00	0.38	3.0	0.63	24.1	0.99	11.3	0.79

TABLE 3: Main Dielectric Relaxation Time τ_D and Longitudinal Relaxation Time τ_L for All Simulated Mixtures and the Experimental Principal Dielectric Relaxation Time (Ref 17)

x_D	0.13	0.35	0.50	0.66	0.81	1.00
τ_D (ps)	46	180	82	47	28	16
τ_{exp} (ps)	30.4	56.8	52.1	41.0	32.6	21.1
τ_L (ps)	0.9	4.8	4.4	1.2	0.8	0.5

Our best fitting parameters for each mixture are shown in Table 2. Values of $a_1 \approx 0$ or $\beta \approx 1$ indicate that the decay is nearly exponential. The results suggest that only at the lowest DMSO concentration is the dipolar relaxation more Debye-like. At $x_D = 0.35$ and 0.50, however, the a_1 parameters are small, but $\beta \approx 0.5$. At this point one cannot tell which function describes better the long time decay of the mixtures' dipolar relaxation. At $x_D = 0.35$, for instance, a difference of about 10% between the biexponential and the stretched exponential functions would appear only at 60 ps, which is 5 times larger than the maximum correlation time considered in the present simulations (i.e, 12 ps). Therefore, like in the methanol−water case,[21] correlation data over much longer time intervals would be necessary in order to know the best functional form of the decay. Such a simulation would be extremely demanding on computer time.

Comparison with available experimental data is most conveniently established through the overall main dielectric relaxation time, τ_D, which is obtained from integrating $\Phi(t)$ with the help of the fitting parameters of Table 2 for all simulated system. The results obtained using the biexponential fits are displayed in Table 3, along with the experimental principal dielectric relaxation time.[11] It can be seen that the simulated dielectric relaxation time τ_D exhibits a nonmonotonic composition dependence, with a maximum around 35% DMSO. The overall trend with composition and the magnitude of τ_D for most compositions are in good agreement with the experimental dielectric relaxation time, which is somewhat surprising given the simplicity of the force fields used in these models. At $x_D = 0.35$ and 0.50, however, the simulations yield a much slower relaxation. A similar effect was also found[16] for the single-particle reorientation time τ_2 and may be due to the fact that the simulations overestimate the magnitude of molecular interactions around 50% composition.[16] It is worth mentioning that estimates for τ_D using the stretched exponential fits are similar to those of Table 3, except between 35 and 66% DMSO, where these estimates are much larger than those shown there.

To further investigate the behavior of the mixture dipolar relaxation, we have separately calculated the self-species and interspecies contributions to the total $\Phi(t)$ time-correlation functions. The results for selected compositions are shown in Figure 6, where we have displayed the functions $\Phi(t)$ (solid lines) obtained from eq 8a, as well as the contributions (eq 8b) $\Phi^{dd}(t)$ (dotted lines, labeled "dd"), $\Phi^{ww}(t)$ (dashed lines, labeled "ww"), and $\Phi^{wd}(t)$ (dashed−dotted lines). For the DMSO-rich mixture (Figure 6a), one notices that the DMSO−DMSO

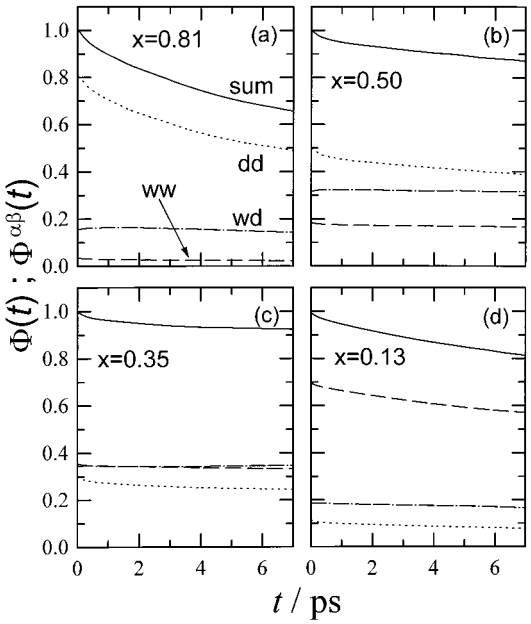

Figure 6. Normalized dipole density correlations $\Phi(t)$ and the self-species and interspecies contributions $\Phi^{\alpha\beta}(t)$ vs time for selected mixtures.

correlations contribute a higher share to the total dipolar relaxation. The water−water and DMSO−water correlations contribute very small amounts to the total $\Phi(t)$, but their relaxation is relatively slow, especially for the $\Phi^{wd}(t)$ because cross-correlations lack the early inertial contributions that comprise an important fast channel of dipolar relaxation. For the equimolar mixture (panel b), the self-species and interspecies terms contribute approximately equal shares to $\Phi(t)$, with $\Phi^{dd}(t)$ being slightly larger than $\Phi^{ww}(t)$, which is not surprising since DMSO has a larger dipolar strength than water. For the water-rich mixture (panel d), the relative contributions of DMSO and water to the total dipolar relaxation have been interchanged when compared to the relaxation of the DMSO-rich mixture. However, there are slight, but important differences between the behavior of these self-species correlations in both mixtures. The most evident one is that $\Phi^{ww}(t)$ in the water-rich mixture (Figure 6d) presents a much slower decay than $\Phi^{dd}(t)$ in the DMSO-rich mixture (Figure 6a). This indicates that addition of DMSO into a sample of water has a much larger impact on the dynamics of the system than adding water into a sample of DMSO. This behavior is reflected in the molecular translational and reorientational dynamics of these mixtures[16] and is also consistent with the static dielectric behavior discussed above. The most noticeable effects of mixing upon the system's dynamics, however, occur at 35% DMSO (Figure 6c). It can be seen that $\Phi^{ww}(t)$ and $\Phi^{dd}(t)$ present smaller decay rates than in the other mixtures and that the interspecies cross-correlations $\Phi^{wd}(t)$ represents now the most important and slowly relaxing component of the dipolar relaxation. The predominance of 1DMSO:2water stable aggregates around this composition is very likely associated with the dynamical behavior found here. Further work, however, is needed to establish a definitive, more quantitative connection between the formation of these aggregates and the dynamics of the mixtures in the rotational-diffusion regime.

Further insight on the way DMSO and water undergo dipolar relaxation upon mixing and the attendant role of the cross-correlations, including those between molecules of the same species and of different species as well, can be gained by comparing the normalized self-species contributions $\Phi^{dd}(t)/\Phi^{dd}$-

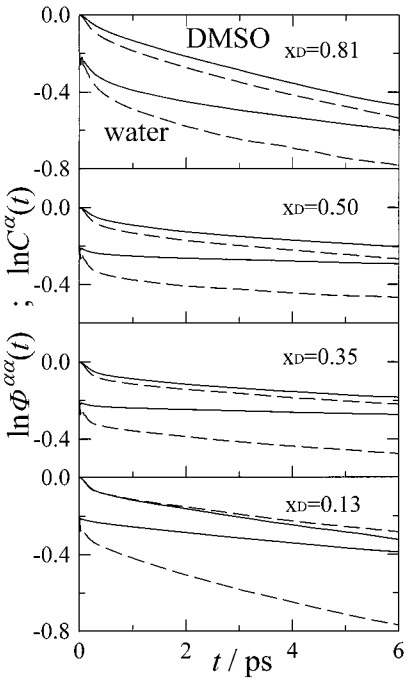

Figure 7. Logarithms of the normalized single-molecule (dashed lines) and collective (solid lines) $k = 0$ dipole time correlations for DMSO and water for selected mixtures. The data for water on each panel have been shifted vertically by −0.2 units for clarity.

(0) and $\Phi^{ww}(t)/\Phi^{ww}(0)$ with the respective single-dipole time correlation function $C^{\alpha}(t) = \langle \hat{u}^{\alpha}(t)\cdot\hat{u}^{\alpha}(0)\rangle$, with α = d, w. The results for the logarithm of these quantities for selected mixtures are displayed in Figure 7, where the collective and single-molecule time correlation functions are depicted by solid and dashed lines, respectively. For clarity, the data for water have been shifted down along the *y*-axes by 0.2 units. The striking feature of these data is that DMSO's collective and single-particle dipole correlation functions present very similar relaxation rates for all mixtures considered, while the decay rates of $\Phi^{ww}(t)/\Phi^{ww}(0)$ and $C^{w}(t)$ are very different. This means that the dynamical cross-correlation between dipoles of the same species in the mixture are not as important for the polarization relaxation rates in the rotational-diffusion regime of DMSO as they are for water. Such cross-correlation between water molecules seems to be important even when water is present in low concentrations ($x_D \sim 80\%$, top panel). In broad terms, the features observed here are qualitatively similar to those found in methanol−water mixtures,[21] with a very distinctive difference, namely, that the cross-correlations of methanol are minor only at the smallest methanol concentrations (∼20% methanol), where most methanol molecules are surrounded by an aqueous environment.

The conclusion that dynamical cross-correlations are not very significant for DMSO can be quantitatively accessed by means of the corresponding micro−macro correlation theorem,[35]

$$\tau_D = \frac{\epsilon(0) - 1}{3y(1 + f)}\tau_S$$

which relates the dielectric relaxation time and the single-dipole reorientational time τ_S through the dynamical cross-correlation factor *f*. Values of $f \approx 0$ indicate that dynamical correlations between dipoles on distinct molecules are negligible. Using $\tau_D = 16$ ps, obtained from the present simulations for pure DMSO (Table 2), and $\tau_S = 8.4$ ps, obtained from our earlier work,[31a] we obtain $f \approx 0.25$. Although not negligible, this value is roughly

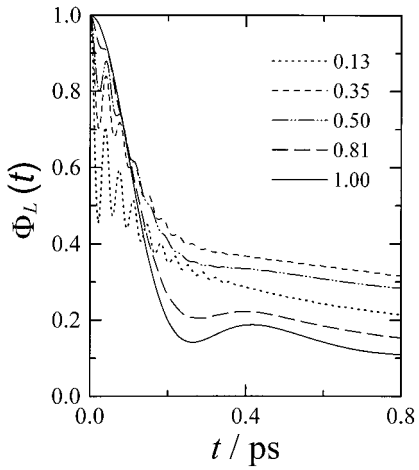

Figure 8. Normalized longitudinal $\Phi_L(\mathbf{k},t)$ functions vs time for each simulated system evaluated at the corresponding smallest nonzero wavevector $k = 2\pi/B$.

5 times smaller than that found for water[30] or methanol,[30,41] two well-known associating liquids. Dynamical cross-correlation factor similar to DMSO's have been found for acetonitrile.[42]

The dynamical behavior described above is consistent with the structural characteristics of the mixtures as given by the dipole−dipole spatial correlation functions $h_{dd}^{110}(r)$ and $h_{ww}^{110}(r)$ of last section and also by site−site pair distribution functions,[4,14−16] which clearly show that water presents an increasing tendency of agglomerating as DMSO is added into the system, whereas the spatial distribution of DMSO goes relatively little affected by the presence of water. Interestingly, the bottom panel of Figure 7 indicates that when small amounts of DMSO is placed in an aqueous environment, its collective dipole time correlation relaxes with a slightly higher decay rate than the single-dipole counterpart $C^{d}(t)$.

B. Longitudinal Correlations. The longitudinal dipolar relaxation is an important quantity to be investigated from the theoretical viewpoint because of its close relationship to the solvation dynamics response of polar liquid environments.[49] The use of the *k*-dependent longitudinal solvent polarization fluctuations instead of the experimental frequency-dependent dielectric permittivity $\epsilon(\omega)$ in modeling the solvents' response to perturbations in solute−solvent electrostatic interactions allows construction of theories[49] for the solvation response, $S(t)$, which go beyond the continuum dielectric treatment by approximately including the dependence of $S(t)$ on the solvent's proximity to the solute and on its translational dynamics. Recently, Day and Patey[26] and Laria and Skaf,[27] have made independent studies of the ionic solvation dynamics in DMSO−water mixtures, which provides then additional motivation to inspect the behavior of the longitudinal dipole density relaxation.

The results for $\Phi_L(\mathbf{k},t)$ evaluated at the smallest wavevector attainable in the simulations, $k_1 = 2\pi/B$, for all simulated systems are displayed in Figure 8 (the curves are labeled according to their mole fraction of DMSO). Figure 8 shows that the librational oscillations are very prominent for mixtures rich in water but that pure DMSO (solid line, bottom panel) also exhibits librational motions with a much larger period of oscillation. It can be noticed that the mixed solvents present slower longitudinal relaxation than pure DMSO, the most sluggish of the two cosolvents. This behavior was also seen the $k = 0$ dipole density time-correlation, but here the effects are more pronounced due to the limited role of rotational-diffusion relaxation channels in the $\Phi_L(\mathbf{k},t)$ functions. Similar behavior occurs in methanol−water, but the variation of the

decay rate with composition follows distinct trends, which can be traced back to the differences between the short-time, inertial relaxation of methanol and DMSO and the very distinct way these molecules interact with water.

The overall longitudinal relaxation time, τ_L, defined as the time integral of the $\Phi_L(\mathbf{k},t)$ functions from zero to infinity, may prove to be a useful estimate for the time scale of solvation dynamics in these environments. The resulting τ_L values for each simulated state are shown in Table 3. Their magnitudes are much smaller than τ_D, as established on fundamental theoretical grounds,[35,36] but here too one sees a nonmonotonic behavior with a maximum around 35% DMSO. Despite the similarities between the $\Phi_L(\mathbf{k},t)$ and the solvation response $S(t)$ for the creation of an ion in these mixtures,[27] the overall relaxation times turned out very different. This behavior can be rationalized in terms of the specificity of the ion−solvent interactions, which are obviously absent here. The solvation of a monatomic ion in these mixtures is characterized by a well-defined first solvation shell of variable composition, which may be more or less structurally tight depending on the sign of the ionic charge and composition of the mixture,[27] so that the time scales for solvent particle exchange between outer and first solvation shells which take place during the solvation dynamics[26] may not be directly associated with the mixture's bulk dynamical behavior. We expect, however, a much closer correspondence between τ_L and the overall solvation times in these mixtures if the solute−solvent interactions are not very specific with either of the constituents. This may likely be the case in time-dependent fluorescence spectroscopy given that real chromophores typically used in solvation dynamics experiments are large, bulky molecules with low charge density on their atomic sites.[25,50]

We close this section by discussing the intra- and interspecies contributions to the total longitudinal dipolar relaxation (solid lines), which are depicted in Figure 8 for some compositions. The contributions from DMSO, water, and the water−DMSO cross-correlations are shown by dotted, dashed, and dotted-dashed lines, respectively. The cross-correlation data have been multiplied by a factor of $-1/2$ in order to set all curves on similar plotting ranges. In all four panels, it can be noticed that the cross-correlations $\Phi_L^{wd}(\mathbf{k},t)$ are negative and free of initial inertial decay and librational oscillations.[51] The fast relaxation of $\Phi_L(\mathbf{k},t)$ results in part by the partial cancelation of the self- and cross-correlations between the molecular species, which is significantly more effective in mixed solvents than in pure liquids, as discussed elsewhere.[21] By comparing the $t = 0$ and $t = 0.8$ ps values of $\Phi_L^{ww}(\mathbf{k},t)$ and $\Phi_L^{dd}(\mathbf{k},t)$, one notices that $\Phi_L^{ww}(\mathbf{k},t)$ relaxes at slower rates than the DMSO−DMSO part $\Phi_L^{dd}(\mathbf{k},t)$, except for the most diluted mixture in DMSO (panel d), where the reverse is true. The data also reveal that the interspecies cross-correlation $\Phi_L^{wd}(\mathbf{k},t)$ is the slowest relaxing component. At 35% DMSO, both $\Phi_L^{ww}(\mathbf{k},t)$ and $\Phi_L^{dd}(\mathbf{k},t)$ have similar initial values and relax nearly at the same rate.

V. Frequency Spectra and Absorption Coefficient

In this section, we investigate the experimentally accessible far-infrared (FIR) absorption spectra,[28,35,52] which portray the system's high-frequency molecular motions. The frequency-dependent quantities of interest here are obtained from the numerical Fourier cosine transforms of the single-dipole and dipole density time correlation functions, where biexponential fits of the form given in eq 13 have been used for the long-time portions of the time-correlation functions in order to aid the numerical transforms.

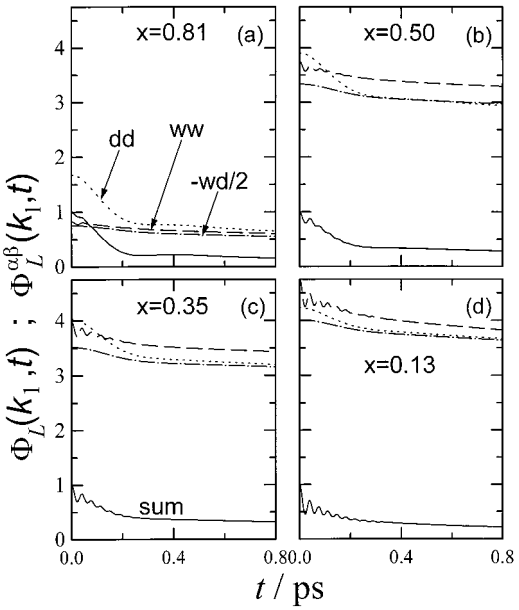

Figure 9. Normalized longitudinal $\Phi_L(\mathbf{k},t)$ function (solid line) evaluated at $k = 2\pi/B$ and the self-species and interspecies contributions $\Phi_L^{dd}(\mathbf{k},t)$ (dotted line), $\Phi_L^{ww}(\mathbf{k},t)$ (dashed line), and $\Phi_L^{dw}(\mathbf{k},t)$ (dashed−dotted line) vs time for selected mixtures. The cross-correlation $\Phi_L^{dw}(\mathbf{k},t)$ has been multiplied by a factor of $-1/2$ for clarity.

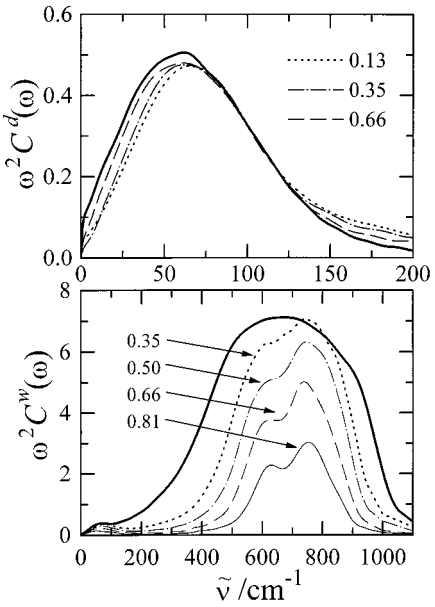

Figure 10. Frequency spectra for the single-dipole time-correlation functions for DMSO (top panel) and water (bottom panel) in the pure liquids (thick lines) and selected mixtures. The curves are labeled according to x_D. The spectra for water molecules are multiplied by water's mole fraction $1 - x_D$ for clarity sakes.

Results for the frequency spectra of DMSO and water single-dipole time-correlation functions for selected mixtures and the pure liquids are shown in Figure 10 in the form $\omega^2 C^\alpha(\omega)$ vs the wavenumber, $\tilde{\nu} = \omega/(2\pi c)$. The top and bottom panels show results for DMSO and water molecules, respectively, where the lines are labeled according to x_D. The thick lines are for the pure liquids. For clarity, the spectra in the lower panel (water's single dipole) have been multiplied by the corresponding mole fraction of water, $1 - x_D$. It is apparent from the upper panel of Figure 10 that the librational band of the individual DMSO dipoles, peaked around 65 cm^{-1}, remains largely unaffected by the presence of water even in the mixtures with lowest fractions

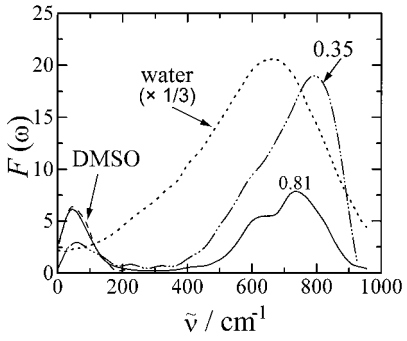

Figure 11. Simulated far-IR spectra for the pure liquids and two selected mixtures. Pure DMSO: dashed line; $x_D = 0.81$: solid line; $x_D = 0.35$: dashed−dotted line. Pure water: dotted line. The latter has been divided by a factor of 3 for clarity.

of DMSO. This behavior is in contrast with the rotational-diffusion dynamics of DMSO molecules, which is strongly dependent on the mixture's composition. The $C^w(\omega)$ data (lower panel), on the other hand, show the intriguing impact DMSO has on the librational motion of water molecules in the mixtures. It can be seen that the librational band of water, characterized by a broad peak centered around 700 cm^{-1} in the pure liquid, is gradually separated into two submaxima as the mole fraction of DMSO increases. At 81% DMSO, the submaxima are well-resolved and centered at 630 and 750 cm^{-1}. We have shown recently that at this composition, most water molecules are found as aggregates of composition 2DMSO:1H_2O,[16] and we have attributed this deconvolution of the spectrum to the presence of such complexes. As we shall see shortly, the origin of these two submaxima can be rationalized in terms of the relaxation modes of the angular velocities of water along the principal axes of motion. In passing, we would like to point out that, for all systems considered, the second submaximum (∼750 cm^{-1}) reaches the rightmost position (highest frequency) when $x_D = 0.35$, but this effect is more clearly seen in the far-IR spectra, which we discuss next.

In the single-particle spectra of Figure 10, the self-species and intraspecies cross-correlations are left out. To provide a closer connection with experimental far-IR spectroscopy, we have calculated the absorption coefficient $\alpha(\omega)$ through eq 11 and the collective dipole time correlation at $k = 0$. The far-IR spectra are conveniently shown here as $F(\omega) = \alpha(\omega)\, n(\omega)/[\epsilon(0) - 1]$ vs wavenumber $\tilde{\nu}$ (Figure 11). The data for pure water (dotted line) have been divided by a factor of 3 in order to set all curves on similar plotting ranges. The spectra for pure DMSO, and for mixtures with $x_D = 0.35$ and 0.81 are depicted by dashed, dashed−dotted, and solid lines, respectively. Results for $\alpha(\omega)$ in units of Np·cm^{-1} are readily recovered by multiplying the data shown by the corresponding values of $\epsilon(0) - 1$, since $n(\omega) \approx 1$ in the frequency range of interest. Centered around 50 cm^{-1}, one notices the main librational relaxation of DMSO reflected in both the mixtures and the pure liquid.[53] Like in the single-particle spectra (Figure 10, upper panel), the band associated with the librational motions of DMSO are little affected by the surrounding water molecules. The far-IR spectrum of pure SPC/E water (dotted line) presents its characteristic, broad librational band peaked at ∼680 cm^{-1}. At 35% DMSO, the band peaks at 800 cm^{-1} and a small shoulder starts to develop around 600 cm^{-1}. For the other mixtures (data not shown, except for $x_D = 0.81$), the band maxima are always located at frequencies smaller than 800 cm^{-1}. The fact that the characteristic librational peak due to water molecules has changed from 680 to about 800 cm^{-1} in going from pure water to a mixture with 35% DMSO is an

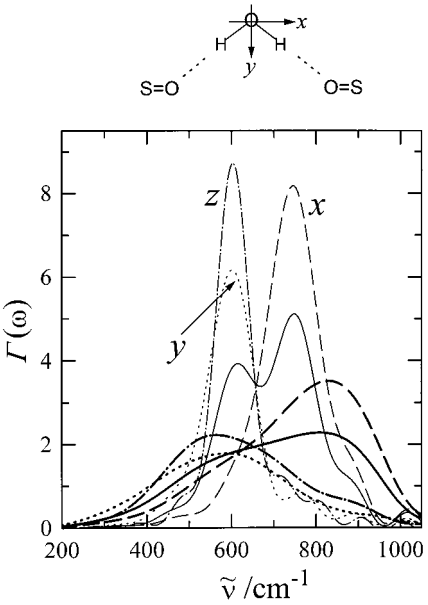

Figure 12. Frequency spectra of the normalized time-correlation functions for the components of the water molecules' angular velocity along the principal axes of inertia in pure water (thick lines) and at $x_D = 0.81$. The curves are labeled according to the set of molecular axes shown. Solid lines depict the spectra for the normalized total angular velocity. The drawing is a schematic of the 2DMSO:1water H-bonded aggregate.

indication that the fast molecular reorientational motions of water molecules are significantly more hindered in this mixture than in the other microenvironments considered here. In the far-IR and single-particle spectra, this effect can be linked to the existence of strong H-bonded molecular aggregates of composition 1DMSO:2water, given that in this frequency range the dielectric loss spectrum is mainly governed by short-ranged structural correlations, as demonstrated by Madden and Kivelson.[35] It has been shown by MD simulations[4,15,16] and neutron scattering experiments[15] that these aggregates do not disrupt the tetrahedral order of water but make it stiffer because the DMSO−water H-bond is somewhat stronger than the water−water bonds.

For the DMSO-rich mixture ($x_D = 0.81$), the librational band of water presents the distinctive, double-humped shape, where the two submaxima around 630 and 750 cm^{-1} are still clearly identified, despite the changes in the band shape compared to the single-particle spectrum. The present results thus suggest that measurements of the far-IR absorption coefficient could be used to probe the existence of 2DMSO:1H_2O molecular aggregates we have discussed above. Since there is no ubiquitous experimental evidence for this type of association, it would be interesting to perform far-IR spectroscopy on these mixtures to see whether our theoretical predictions correspond to reality or not.

Finally, we would like to discuss in more detail how DMSO affects the short-time reorientational dynamics of water and investigate which molecular motions give rise to the splitting of water's librational band in DMSO-rich mixtures. For this purpose, we have calculated the frequency spectra $\Gamma^j(\omega)$ for the normalized angular velocity time-correlation functions of water molecules along the principal axes of inertia ($j = x, y, z$). The results are shown in Figure 12 for pure water (thick lines) and the 81% DMSO mixture. Depicted are the spectra for the normalized total angular velocity (solid lines) and the separate components along the x, y, and z principal axes, according to the drawing on top of Figure 12 (the z axis is normal to the

molecular plane; DMSO's methyl groups are not shown). As is well-known, the broad band in the total spectrum for pure water emerges as the overlap of the spectra about the three axes, of which only $\Gamma^x(\omega)$ and $\Gamma^z(\omega)$ would be manifested in the spectrum of dipole reorientational motions for obvious reasons. Notice too that the position of the peaks follows the inverse order of the respective moments of inertia ($I_{xx} < I_{yy} < I_{zz}$). For the DMSO-rich mixture, the total spectrum of water's angular velocity is clearly deconvoluted into two submaxima in the same fashion we already discussed. It can be seen that this stems from the sharpening of the three $\Gamma^j(\omega)$ spectra that takes place when water is mostly surrounded by DMSO. This effect can be understood in the light that the distribution of H-bonds for water molecules in this mixture is sharply peaked, with roughly 80% of the water molecules being doubly H-bonded to two DMSO (see schematic in Figure 12), whereas in pure water the H-bond distribution is much broader.[16]

Further inspection of Figure 12 reveals that the peak positions of $\Gamma^y(\omega)$ and $\Gamma^z(\omega)$ in going from pure water to the DMSO-rich mixture are little affected, while the peak of $\Gamma^x(\omega)$ shifts from about 850 to 750 cm^{-1}, indicating that in the $x_D = 0.81$ mixture the rapid rotations of the water molecule about the x axis are less hindered than in pure water. Once more, this behavior can be rationalized in terms of the molecular aggregate portrayed in Figure 12. The donor character of the depicted water molecule is very similar to that in pure water, where the DMSO oxygen atoms would be replaced by water's. The acceptor character, however, is very distinct from that it would have if plenty of water molecules were available in the system. With practically no H-bonding on its oxygen atom, this water molecule experiences very weak restoring forces off the plane of the sheet, which in turn render rotations about the x axis easier to perform.

VI. Summary and Concluding Remarks

In this paper we have presented and discussed the results of extensive MD simulations aimed at investigating the static and dynamic dielectric behavior of DMSO−water mixtures over the whole composition range. Analyses were performed in terms of the separate contributions from each molecular species, and the role of the cross-correlations, which are usually less accessible experimentally, have been investigated. Special attention has been devoted to unravel the effects of the distinct types of molecular H-bonded aggregates on the static and dynamic dielectric behavior of these mixtures. Our main conclusions are summarized as follows.

A. Static Properties. We find good agreement between the simulated and the available experimental dielectric constant for all compositions. Despite the facts that the intermolecular potentials used here are not fully polarizable and that no adjustment of the parameters has been made, the simulated values for $\epsilon(0)$ are only about 10% too low in comparison with the experimental ones. Unlike methanol−water mixtures, the observed decrease in $\epsilon(0)$ with x_D is due to changes in the dipole−dipole correlations, not because of differences in the dipolar strength of the mixture, as revealed by the decrease in the Kirkwood g factor g_K with increasing DMSO concentration. Analysis of the approximated self-species and interspecies contributions to g_K shows that mixing reduces the g_K^{ww} and g_K^{dd} terms below the values one would expect if the mixing were random, while at the same time it enhances the interspecies cross-correlations g_K^{wd} to a maximum around 35% DMSO. Analysis of the projections $h_{\alpha\beta}^{110}(r)$ in real-space indicates that this enhancement in g_K^{wd} is consistent with the formation of 1DMSO:2water aggregates. For DMSO-rich mixtures ($x_D = 0.81$), we find that $g_K < g_K^{DMSO}$, indicating that a small addition of water into DMSO enhances antiparallel alignment of DMSO dipoles. This behavior is, in turn, consistent with the formation of H-bonded aggregates of the type 2DMSO:1water, and also with experimental observations.

B. Main Dielectric Relaxation. The mixture's overall dielectric relaxation time τ_D is in good agreement with the experimental principal dielectric relaxation time, except for compositions between 35 and 50% DMSO, where the simulations predict significantly higher relaxation times. Despite that, τ_D passes through a maximum around $x_D = 0.35$. In passing, the dielectric relaxation time for the P2 potential of liquid DMSO (Table 2), obtained here for the first time, is a little smaller than the experimental value. This behavior is consistent with the fact that P2 overestimates the diffusion coefficient of DMSO.[31a] Analyses of the self-species and interspecies time correlations show that the water−water and water−DMSO correlations are the slowest relaxing components and that addition of DMSO into water has a much larger impact on the system's dipolar relaxation than adding water into DMSO. This behavior is consistent with the single-molecule translational and reorientational motions studied previously. Comparison between the normalized collective self-species contributions, $\Phi^{ww}(t)/\Phi^{ww}(0)$ and $\Phi^{dd}(t)/\Phi^{dd}(0)$, and the corresponding single-particle time correlations, $C^w(t)$ and $C^d(t)$, shows that dynamical cross-correlations between DMSO molecules in the rotational-diffusion regime are not nearly as important as they are for water for all mixtures considered. This is consistent with the structural properties studied previously and the dipolar symmetry projections $h_{\alpha\beta}^{110}(r)$ discussed here, which reveal that mixing favors "clustering" of water molecules, whereas DMSO preserves the somewhat loose structure it has in the neat state.

C. Longitudinal Relaxation. The behavior the longitudinal dipolar relaxation reveals important differences in the short-time inertial and librational dynamics of the two cosolvents and the nontrivial effect that mixing brings about. The overall longitudinal relaxation time also goes through a maximum around 35% DMSO and the reported values may be useful estimates for the solvation dynamics response times of these mixtures. The separate calculation of the self-species and interspecies contributions indicates that interspecies cross-correlations comprise an important slow component to the longitudinal relaxation of these mixtures.

D. Librational Motions and Frequency Spectra. The fast librational motions of DMSO and water are quite different from each other in the pure liquids and are also very distinctively affected by mixing. The spectrum for DMSO's single-dipole time correlation presents a maximum around 65 cm^{-1} and remains practically unaltered upon mixing, presenting a mild shift toward higher frequencies as water is added. This implies that the environmental changes and the concomitant formation of molecular associations with water molecules actually have little impact on the short-time reorientational dynamics of DMSO molecules in these mixtures. The librational dynamics water, on the other hand, is profoundly affected by the presence of DMSO in ways that differ according to the composition. At $x_D = 0.35$, the single-dipole spectrum of water has apparently a single librational band that peaks with the highest frequency, an indication of the stiffness brought about by the existence of 1DMSO:2water aggregates. For DMSO-rich mixtures, the librational band subdivides into two submaxima centered around 630 and 750 cm^{-1}, which are shown to be due to aggregates of the type 2DMSO:1water. An analysis of the frequency spectra

for the components of the angular velocity of water molecules at $x_D = 0$ and 0.81 reveals how this splitting emerges from the 2:1 complexes. The experimentally accessible, far-IR absorption coefficients have also been calculated from the frequency spectra of the collective dipole time correlations for the pure liquids and the 35 and 81% DMSO mixtures. The band due to DMSO (peaked at $\sim$50 cm^{-1}) does not change its position, whereas the band due to water develops the double-humped appearance as x_D increases, indicating that far-IR spectroscopy or another suitable experimental technique sensitive to water's librational motions could be used to detect the existence of the 2DMSO:1water aggregates suggested by the simulations.

Acknowledgment. Financial support from the Brazilian agencies FAPESP (grant 95/9508-7) and CNPq is very much appreciated. The author also thanks Sergio Vechi for calculating the spectra for the angular velocity time-correlation functions.

References and Notes

(1) Martin, D.; Hanthal, H. *Dimethyl Sulfoxide*; Wiley: New York, 1975.
(2) De la Torre, J. C. *Ann. N. Y. Acad. Sci*. **1983**, *411*, 1.
(3) Safford, G. J.; Schaffer, P. C.; Leung, P. S.; Doebbler, G. F.; Brady, G. W.; Lyden, E. F. X. *J. Chem. Phys.* **1969**, *50*, 2140.
(4) Luzar, A.; Chandler, D. *J. Chem. Phys.* **1993**, *98*, 8160.
(5) Cowie, M. G.; Toporowski, P. M. *Can. J. Chem.* **1964**, *39*, 224.
(6) Fox, F.; Whittingham, K. P. *J. Chem. Soc., Faraday Trans*. **1974**, *75*, 1407.
(7) Tommila, E.; Pajunen, A. *Suomen Kemistil. B* **1969**, *41*, 172.
(8) Gordalla, B. C.; Zeidler, M. D. *Mol. Phys*. **1986**, *59*, 817; **1991**, *74*, 975.
(9) Packer, K. J.; Tomlinson, D. J. *Trans. Faraday Soc*. **1971**, *67*, 1302.
(10) Tokuhiro, T.; Menafra, L.; Szmant, H. H. *J. Chem. Phys*. **1974**, *61*, 2275.
(11) Kaatze, K.; Pottel, R.; Schäfer, M. *J. Phys. Chem.* **1989**, *93*, 5623.
(12) Luzar, A. *J. Chem. Phys.* **1989**, *91*, 3603.
(13) Benjamin, I. *J. Chem. Phys*. **1999**, *110*, 8070.
(14) Vaisman, I. I.; Berkowitz, M. L. *J. Am. Chem. Soc*. **1992**, *114*, 7889.
(15) Soper, A. K.; Luzar, A. *J. Phys. Chem*. **1996**, *100*, 1357; *J. Chem. Phys*. **1992**, *97*, 1320.
(16) Borin, I. A.; Skaf, M. S. *Chem. Phys. Lett*. **1998**, *296*, 125; *J. Chem. Phys*. **1999**, *110*, 6412.
(17) Baker, E. S.; Jonas, J. *J. Phys. Chem*. **1985**, *89*, 1730.
(18) (a) Ferrario, M.; Haughney, M.; McDonald, I. R.; Klein, M. L. *J. Chem. Phys.* **1990**, *93*, 5156. (b) Tanaka, H.; Gubbins, K. E. *J. Chem. Phys.* **1992**, *97*, 2626. (c) Palinkas, G.; Hawlicka, E.; Heinzinger, K. *Chem. Phys*. **1991**, *158*, 65.
(19) Luzar, A. *J. Mol. Liq*. **1990**, *46*, 221.
(20) Skaf, M. S.; Ladanyi, B. M. *J. Chem. Phys*. **1995**, *102*, 6542.
(21) Ladanyi, B. M.; Skaf, M. S. *J. Phys. Chem*. **1996**, *100*, 1368.
(22) Wei, D.; Patey, G. N. *J. Chem. Phys*. **1991**, *94*, 6785.
(23) Chandra, A. *Chem. Phys*. **1995**, *195*, 93.
(24) Hansen, J.-P.; McDonald, I. R. *Theory of Simple Liquids*, 2nd ed.; Academic Press: London, 1969.
(25) Stratt, R. M.; Maroncelli, M. *J. Phys. Chem*. **1996**, *100*, 12981. Maroncelli, M. *J. Mol. Liq.*. **1993**, *57*, 1.
(26) Day, T. J. F.; Patey, G. N. *J. Chem. Phys*. **1999**, *110*, 10937.
(27) Laria, D.; Skaf, M. S. *J. Chem. Phys*. **1999**, *111*, 300.
(28) Böttcher, C. J. F.; Bordewijk, P. *Theory of Electric Polarization II*; Elsevier: Amsterdam, 1978.
(29) Berendsen, H. J. C.; Grigera, J. R.; Straastma, T. P. *J. Phys. Chem*. **1987**, *91*, 6269.
(30) Ladanyi, B. M.; Skaf, M. S. *Annu. Rev. Phys. Chem*. **1993**, *44*, 335.
(31) (a) Skaf, M. S. *J. Chem. Phys*. **1997**, *107*, 7996. (b) *Mol. Phys*. **1997**, *90*, 25.
(32) (a) de Leeuw, S. W.; Perram, J. M.; Smith, E. R. *Annu. Rev. Phys. Chem.* **1986**, *37*, 245. (b) *Proc. R. Soc. London A* **1980**, *373*, 27. (c) *Proc. R. Soc. London A* **1980**, *373*, 57.
(33) (a) Allen, M. P.; Tildesley, D. J. *Computer Simulation of Liquids*; Clarendon: Oxford, U.K., 1987. (b) Hockney, R. W. *Methods Comput. Phys.* **1970**, *9*, 136.
(34) Ciccotti, G.; Ryckaert, J.-P. *Comput. Phys. Rep.* **1986**, *4*, 345.
(35) Madden, P. A.; Kivelson, D. *Adv. Chem. Phys*. **1984**, *56*, 467.
(36) Stell, G.; Patey, G. N.; Høye, J. S. *Adv. Chem. Phys*. **1981**, *48*, 183.
(37) Borysow, J.; Moraldy, M.; Frommhold, L. *Mol. Phys*. **1985**, *56*, 913.
(38) Guillot, B. *J. Chem. Phys*. **1991**, *95*, 1543; Guillot, B.; Guissani, Y. In *Collision- and Interaction Induced Spectroscopy*; Tabisz, G. C., Neuman, M. N., Eds.; Kluwer: Amsterdam, 1995.
(39) Flyvberg, H.; Petersen, H. G. *J. Chem. Phys*. **1989**, *91*, 461.
(40) Reddy, M. R.; Berkowitz, M. L. *Chem. Phys. Lett*. **1989**, *155*, 173.
(41) Skaf, M. S.; Fonseca, T.; Ladanyi, B. M. *J. Chem. Phys*. **1993**, *98*, 8929.
(42) Edwards, D. M. F.; Madden, P. A.; McDonald, I. R. *Mol. Phys*. **1984**, *51*, 1141.
(43) Amey, R. L. *J. Phys. Chem*. **1968**, *72*, 3358.
(44) Luzar, A.; Soper, A. K.; Chandler, D. *J. Chem. Phys*. **1993**, *99*, 6836.
(45) Bertolini, D.; Cassettari, M.; Salvetti, G.; Tombari, E.; Veronesi, S. *J. Non-Cryst. Solids* **1991**, *131*, 1169.
(46) Bertolini, D.; Cassettari, M.; Salvetti, G. *J. Chem. Phys*. **1983**, *78*, 365.
(47) Mashimo, S.; Kuwabara, S.; Yagihara, S.; Higasi, K. *J. Chem. Phys*. **1989**, *90*, 3292.
(48) (a) Ediger, M. D.; Angell, C. A.; Nagel, S. R. *J. Phys. Chem*. **1996**, *100*, 13200. (b) Shlesinger, M. F. *Annu. Rev. Phys. Chem*. **1988**, *39*, 269.
(49) (a) Raineri, F. O.; Resat, H.; Perng, B.-C.; Hirata, F.; Friedman, H. L. *J. Chem. Phys*. **1994**, *100*, 1477. (b) Friedman, H. L.; Raineri, F. O.; Hirata, F.; Perng, B.-C. *J. Stat. Phys.* **1995**, *78*, 239.
(50) Kumar, P. V.; Maroncelli, M. *J. Chem. Phys*. **1995**, *103*, 3038.
(51) Kivelson, D.; Friedman, H. L. *J. Phys. Chem*. **1989**, *93*, 7026.
(52) Madden, P. A. In *Molecular Dynamics Simulations of Statistical Mechanics Systems*; Ciccotti, G., Hoover, W. G., Eds.; North-Holland: Bologna, 1986.
(53) We are unaware of any published experimental far-IR spectrum for pure DMSO in the neighborhood of its librational band. However, Bulkin[54] and Guillot et al.[55] quote (without showing the spectra) far-IR bands peaked at 83 and 88 cm^{-1}, respectively. The present result thus indicates that the P2 potential underestimates the frequency of the collective librational band of DMSO (i.e., 50 cm^{-1}) compared to these experimental measurements.
(54) Bulkin, B. J. *Helv. Chim. Acta* **1969**, *52*, 1348.
(55) Guillot, B.; Marteau, Ph.; Obriot, J. *J. Chem. Phys*. **1990**, *93*, 6148.